PERGAMON

International Journal of Heat and Mass Transfer 46 (2003) 1049–1061

International Journal of HEAT and MASS TRANSFER

www.elsevier.com/locate/ijhmt

Local heat/mass transfer and flow characteristics of array impinging jets with effusion holes ejecting spent air

Dong-Ho Rhee, Pil-Hyun Yoon, Hyung Hee Cho *

Department of Mechanical Engineering, Yonsei University, 134, Shinchon-Dong Seodaemun-ku, Seoul 120-749, South Korea

Received 30 December 2001; received in revised form 28 August 2002

Abstract

The present study investigates the effects of spent air flows with and without effusion holes on heat/mass transfer on a target plate for array impinging jets. For a conventional type of array impinging jets without effusion holes, the spent air of the injected jets forms a cross-flow within the confined space and affects significantly the downstream jet flow. The injection plate of array impinging jets is modified having effusion holes to prevent the cross-flow of the spent air where the spent air is discharged through the effusion holes after impingement on the target plate. A naphthalene sublimation method is employed to determine local heat/mass transfer coefficients on the target plate using a heat and mass transfer analogy. The flow patterns of the array impinging jets are calculated numerically and compared for the cases without and with the effusion holes. For small gap distances, heat/mass transfer coefficients without effusion holes are very non-uniform due to the strong effects of cross-flow and re-entrainments of spent air. However, uniform distributions and enhancements of heat/mass transfer coefficients are obtained by installing the effusion holes. For large gap distances, the effect of cross-flow is weak and the distributions and levels of heat/mass transfer coefficients are similar for both cases.

1. Introduction

Jet impingement is a common method of heating or cooling solid surfaces. Heat transfer under impinging jet is generally superior to that achieved with typical convective heat transfer methods. The impingement cooling jet has an advantage that it is easy to adjust the location of interest and remove a large amount of heat effectively. In many industrial systems, including high temperature gas turbines, paper and glass manufacturing plants and high density electrical and electronic equipment, impinging jets are used to cool, heat or dry a surface. It is necessary to use multiple jets to cool or heat a large area in many applications.

The arrays of impingement jets have two major differences from a single jet: One is the interference between adjacent jets prior to their impingement on the surface. The other is the collision of the surface flows (wall jets) associated with adjacent impinged jets [1]. Martin [2], Downs and James [3], Jambunathan et al. [4] and Viskanta [5] reviewed extensively the previous studies of single/array jet impingement heat transfer.

For the conventional array impinging jets, a cross-flow is formed by the spent air from the impinging jets in a confined space, and the amount of the cross-flow increases as the flow moves downstream. Turbulence intensity of impinging jets is increased because the cross-flow disturbs impinging jets at downstream region. Therefore, the local heat/mass transfer rate around the stagnation region is enhanced. However, at the mid-way region, the heat/mass transfer coefficients are decreased because the thermal boundary layer develops in the cross-flow at this region and flow pattern is similar to the duct flow [6]. Therefore, the heat/mass transfer coefficients are non-uniform over the overall impingement surface, and this non-uniformity can induce thermal stress problem on the target plate.

One possible method to reduce the adverse effects of cross-flow is to install the effusion holes and extract the spent air through the effusion holes. Cho and Goldstein [7] and Cho and Rhee [8] investigated the effect of hole

* Corresponding author. Tel.: +82-2-2123-2828; fax: +82-2-312-2159.

E-mail address: hhcho@yonsei.ac.kr (H.H. Cho).

0017-9310/03/$ - see front matter
PII: S0017-9310(02)00363-0

Nomenclature

d	exit diameter of injection hole
D	effusion hole diameter
D_{naph}	naphthalene vapor diffusivity in air
H	gap distance between injection and target plates
h	local heat transfer coefficient
h_m	local mass transfer coefficient
l	thickness of injection plate
$\dot{m}$	mass transfer rate per unit area
Nu	Nusselt number
P_{cham}	plenum chamber gage pressure
Pr	Prandtl number
Re_d	Reynolds number based on hole diameter and mean velocity of the jet
S	center-to-center spacing between injection holes
Sc	Schmidt number
Sh	local Sherwood number, Eq. (2)
$\overline{Sh}$	spanwise-averaged Sherwood number, Eq. (3)
$\overline{\overline{Sh}}$	overall-averaged Sherwood number, Eq. (4)
x, y	coordinate system, Fig. 2
z	vertical distance from the target surface, Fig. 2
ΔP	pressure drop through the test section
Δy	naphthalene sublimation depth

Greek symbols

$\Delta\tau$	time interval during experiment
ρ_s	density of solid naphthalene
$\rho_{v,w}$	naphthalene vapor density on the surface
$\rho_{v,\infty}$	naphthalene vapor density of the injected jet

arrangements on local heat/mass transfer characteristics for the array jet impingement with spent air removal through the effusion holes on the target plate. They found that the high transfer rate is induced by strong secondary vortices and flow acceleration, and the overall transfer rate is approximately 45–55% higher than that for impingement cooling alone. Rhee et al. [9] investigated the local heat/mass transfer characteristics with various cross-flow ratios for the impingement/effusion cooling system. Also, Hollworth and Dagan [10] and Hollworth et al. [11] measured the average and local heat transfer coefficients of arrays of turbulent air jets impinging on perforated target surfaces, and reported that arrays with staggered vents consistently yield 20–30% higher heat transfer rates than do the impinging jets on the solid plates.

However, in many applications of array jet impingement, it is difficult to remove the spent air through the target plate. Therefore, the discharge of spent air through the injection plate by installing effusion holes is a possible method to reduce the effect of cross-flow and enhance the heat transfer on the target plate.

Huber and Viskanta [12] studied the effect of spent air exit in the orifice plate on the local and average heat transfer for 3×3 square array jet with 2×2 square spent air exit using the liquid crystal technique. Also, they examined the effects of the gap distances ($H/D = 0.25$, 1.0, 6.0) and the Reynolds numbers (3500–20,400). They found that the interaction of adjacent impinged jets is reduced by spent air and the heat transfer on target plate is more enhanced.

The present study investigates local heat/mass transfer and flow characteristics on the target plate for arrays of impinging jets with different types of spent air exit; conventional array jets (array jets without effusion holes) and array jets with effusion holes (spent air exit) on the injection plate, and compares the results for various gap distances between the injection and target plates.

A naphthalene sublimation method is used to measure local heat/mass transfer coefficients on the target plate. This technique eliminates the conduction and radiation errors inherent in heat transfer experiments. The surface boundary condition is analogous to an isothermal surface in a corresponding heat transfer problem. The details of naphthalene sublimation method is presented by Goldstein and Cho [13].

The analysis of flow field is needed to understand local heat/mass transfer characteristics on the target plate. Therefore, surface flow visualization and numerical simulations using a commercial program (FLUENT) are performed to investigate the flow characteristics between the injection and target plates.

2. Experimental apparatus and procedure

2.1. Experimental apparatus

Fig. 1 shows the experimental apparatus which consists of a blower, a heat exchanger, an orifice flowmeter, a plenum chamber, and a test section with array of jet nozzles. Air is supplied by the inverter-controlled blower (3.7 kW). The temperature of the jet air is kept constant through the heat exchanger with a constant-temperature reservoir. The flow rate is measured using the orifice flowmeter. A baffle and a honeycomb are inserted in the plenum chamber to insure a uniform flow through each injection hole. The temperature of the flow in the plenum chamber is measured by T-type thermocouples.

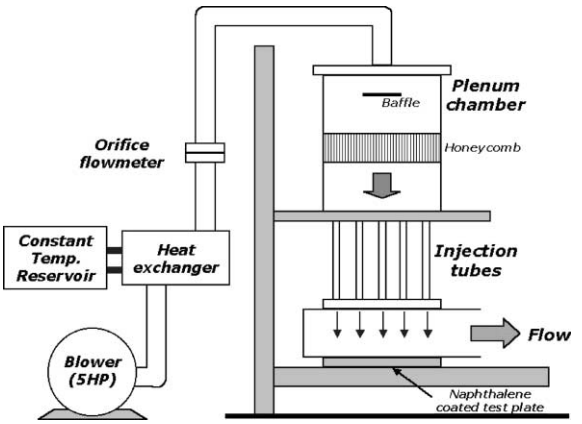

Fig. 1. Schematic view of experimental apparatus.

The air in the plenum chamber is distributed through tubes, and injected to the target plate through the injection holes in a plate. The length of tube is set to equal to obtain equal pressure drop through the tubes.

Test section for conventional array impinging jets with downstream spent air exit (without effusion holes) is shown in Fig. 2(a). The injection holes are positioned in a square arrangement and have contracted geometry at the middle of the injection plate. The inlet diameter of injection hole is 15 mm and the exit diameter (d) of injection hole is 10 mm. The thickness of injection plate is 20 mm ($l/d = 2.0$), and the hole-to-hole spacing is 60 mm ($S/d = 6.0$). The jet array is enclosed by three sidewalls which guide cross-flow of the spent air to maximize the effect of cross-flow on array jet impingement. Thus, the cross-flow of the injected jets is formed and flows in one-direction and the downstream jets are injected into the cross-flow. The sidewalls are positioned at a distance of $S/2$ (symmetry plane) from the outermost jet holes, so that the hole array simulates infinite numbers of jets.

Fig. 2(b) shows the test sections for array impinging jets with effusion holes on the injection plate. The jets are injected into the chamber (closed space) and discharged only through the effusion holes on the injection plate. Twenty-five effusion holes are installed on the injection plate and centered among four injection holes as shown in Fig. 2(b). The diameter of effusion hole (D) is 15 mm, and hole-to-hole spacing is the same as that of injection hole ($S/D = 4.0$; $S/d = 6.0$).

The spacing between the injection and target plates (H) is changed from $H/d = 0.5$ to $H/d = 10$, and Reynolds number of an injected jet is set to $Re_d = 10{,}000$ for the present study. As shown in Fig. 2, a naphthalene coated test plate is installed on the target plate to measure local heat/mass transfer coefficients, and the dimension of the naphthalene coated surface is 300 mm ($30d$) by 150 mm ($15d$). A T-type thermocouple is installed inside the test plate to measure the temperature of naphthalene surface.

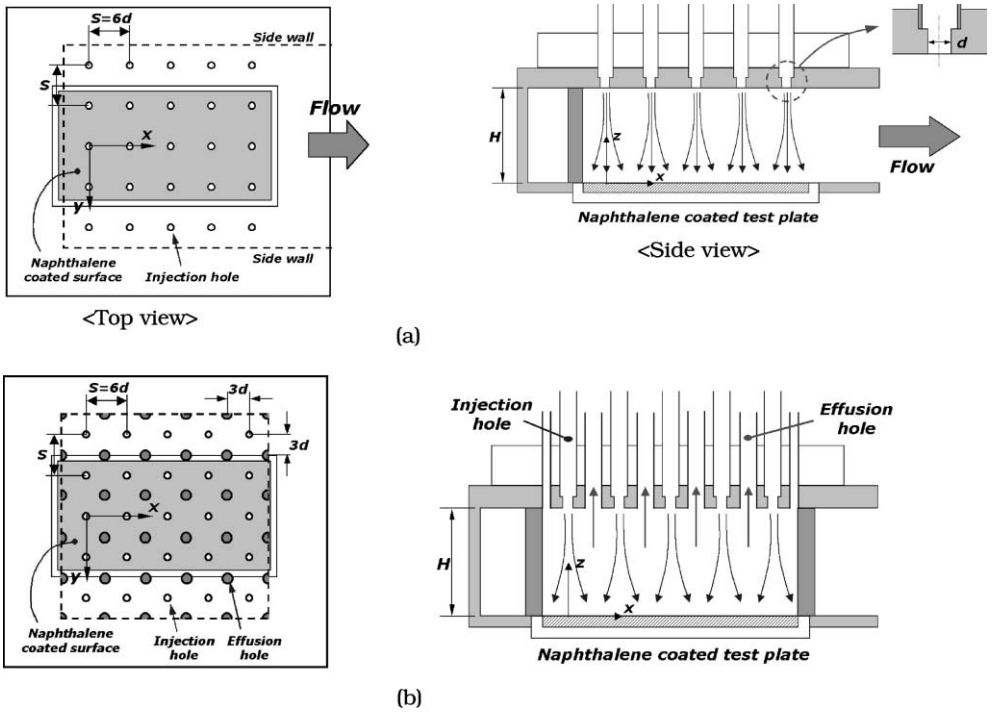

Fig. 2. Schematic views of test section and hole arrangement: (a) without effusion holes and (b) with effusion holes.

Table 1
Pressure drop in test section for array impinging jet without effusion holes at $Re_d = 10{,}000$

H/d	Pressure drop without orifice ($\Delta P/P_{cham}$, %)	Pressure drop with orifice ($\Delta P/P_{cham}$, %)
0.5	69.5	4.8
1.0	35.0	1.4
2.0	13.4	0.6
4.0	5.8	–

For the array impinging jet without the effusion holes, the pressure drop through the test section is generated due to the cross-flow effect. The pressure drop is estimated by measuring the static pressure difference between at the upstream region ($x/d = -3.0$) and the exit region ($x/d = 27.0$). For the small gap distances ($H/d = 0.5$ and 1.0), the static pressure at the upstream region is higher than that at the downstream region and the ratios of the pressure drop to the static pressure in the plenum chamber are 69.5% and 35.0%, respectively. Therefore, the velocity distribution of impinging jets would be non-uniform for the small gap distances. To reduce this problem, thick orifices of which the inner diameter is 4 mm and the length is 50 mm are inserted in the tubes connected to the plenum chamber and test section. With the orifices in the tube, as shown in Table 1, the ratio of pressure drop is decreased to 4.8% and 1.4% for $H/d = 0.5$ and 1.0, respectively. Therefore, it can be assumed that a uniform array jet impingement is obtained in the present study.

For the velocity measurement at the injection hole exit, a hot-wire anemometer (TSI-IFA300) which is a constant-temperature type with I-type sensor is used. The hot wire probe is carried by three-axis traverse controlled by PC. The sampling rates are 4000 Hz and the number of sampled data is 4096 points and a low pass filter of 2000 Hz is used for the measurement.

2.2. Data acquisition

In order to obtain local mass transfer coefficients, the profile of the naphthalene surface coated on the test plate is scanned by an automated surface measuring system before and after exposure to the air flow. Sublimation depth during the run is calculated from the difference of the surface profiles. Details of the measuring system are presented by Cho and Rhee [8].

2.3. Heat/mass transfer coefficient

The local mass transfer coefficient is defined as:

$$h_m = \frac{\dot{m}}{\rho_{v,w} - \rho_{v,\infty}} = \frac{\rho_s(\Delta y/\Delta\tau)}{\rho_{v,w}} \tag{1}$$

since impingement jet flow contains no naphthalene, $\rho_{v,\infty} = 0$, in the present study. Therefore, the mass transfer coefficient is calculated from the local sublimation depth of naphthalene (Δy), run time ($\Delta\tau$), density of solid naphthalene (ρ_s), and naphthalene vapor density ($\rho_{v,w}$). The naphthalene vapor pressure is obtained from a correlation of Ambrose et al. [14]. Then the naphthalene vapor density, $\rho_{v,w}$, is calculated from the perfect gas law.

The Sherwood number can be expressed as:

$$Sh = h_m d/D_{naph} \tag{2}$$

D_{naph} is based on the discussion of naphthalene properties given by Goldstein and Cho [13].

The spanwise-averaged Sh is obtained by a numerical integration:

$$\overline{Sh} = \frac{\int_0^{S/2} Sh\,dy}{S/2} \tag{3}$$

In addition, the overall-averaged Sh for five rows is calculated as:

$$\overline{\overline{Sh}} = \frac{\int_{x/d=-3}^{x/d=26} \overline{Sh}\,d(x/d)}{29} \tag{4}$$

The mass transfer coefficients can be converted to the heat transfer coefficients using the heat and mass transfer analogy [15]. The Prandtl number is 0.71 for air and the Schmidt number is 2.28 for the naphthalene vapor in air at 25 °C. Since the experiments are conducted at room temperature, the Lewis number (Pr/Sc) for this study is about 0.307.

$$\frac{Nu}{Sh} = \left(\frac{Pr}{Sc}\right)^{0.4}, \quad Nu = 0.624\,Sh \tag{5}$$

Uncertainty values of the Sherwood number and the mass transfer coefficient using Kline and McClintock's [16] method for single sample experiments, considering the measured temperature, depth, position and correlation equations, are within 6.2% and 5.4% in the entire operating range of the measurement, respectively, based on a 95% confidence interval.

These uncertainties are attributed mainly to the uncertainty of properties of naphthalene, such as the naphthalene saturated vapor pressure (5.1%), and diffusion coefficient of naphthalene vapor in the air (3.0%). However, uncertainty due to the sublimation depth measurement is only 0.7%. The other uncertainties are 0.12% and 1.1% for T_w and ρ_s, respectively.

The major uncertainties in the saturated vapor pressure and naphthalene vapor diffusivity result mainly from temperature values in each correlation. Thus, the error can be reduced significantly if each experimental test is conducted in the same temperature condition.

2.4. Numerical analysis

A numerical analysis using a commercial program (FLUENT V5.4) is performed for the array impinging jets without and with effusion holes in order to understand the flow patterns. FLUENT is based on a finite volume method with SIMPLE algorithm and is used widely for general flow problems. The computational domains are modeled by the geometries used in the experiment, and the operating conditions are equal to those of the experiments.

The computation domain grids are created using the GAMBIT solid modeling and have non-uniform meshes with fine grids in the regions of sharp velocity gradients. Various grids are used to verify the grid independence of the solution. To reduce grid sizes and calculation times, the symmetry boundary conditions are applied to the sidewalls (array jets without effusion holes) or cell

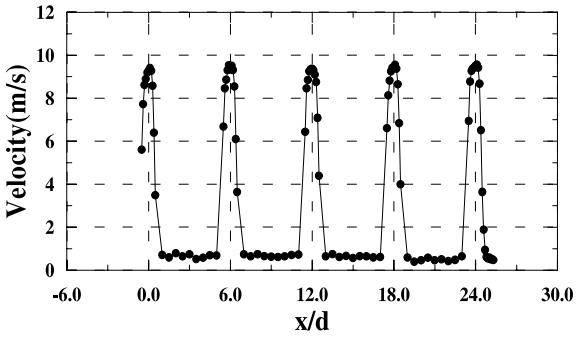

Fig. 3. Velocity profile at the nozzle exit for $Re_d = 5000$.

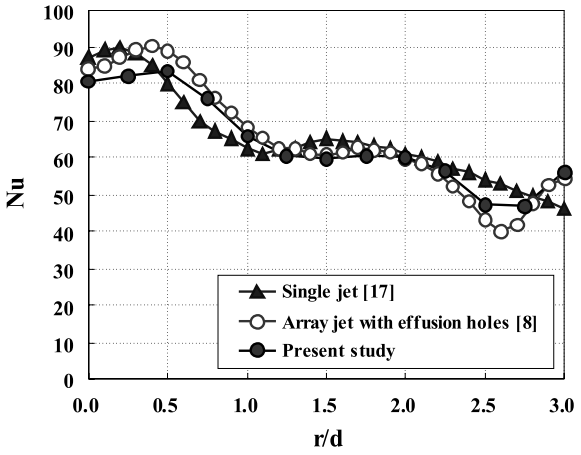

Fig. 4. Comparison of local Nu number for impinging jet with other results for $H/d = 2.0$ and $Re_d = 10{,}000$ along $y/d = 0.0$.

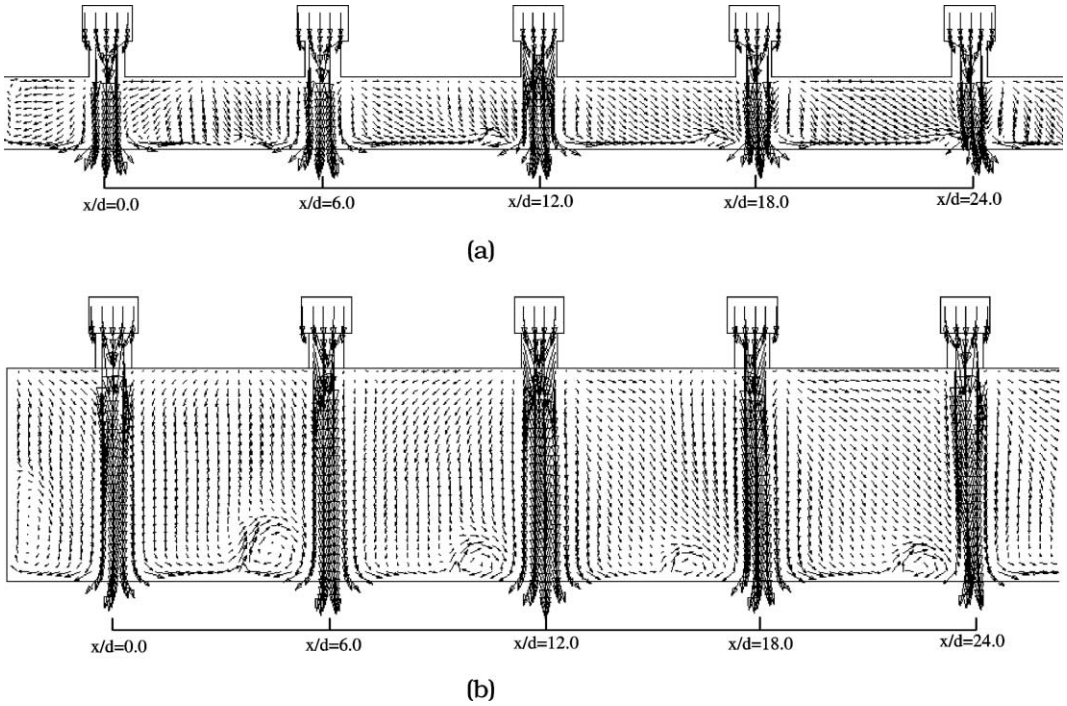

Fig. 5. Velocity vector plots at center-plane for array impinging jets without effusion holes at $Re_d = 10{,}000$. (a) $H/d = 2.0$ and (b) $H/d = 6.0$.

boundary (array jets with effusion holes), and the number of grid points is about 200,000. The conditions of numerical calculation are steady, three-dimensional and turbulent flow using a Reynolds stress turbulence modeling (RSM) with a standard wall function for near wall region. The Reynolds number (Re_d) is fixed at 10,000 for the numerical calculations.

3. Results and discussion

3.1. Qualification tests

The qualification tests are performed to ensure the symmetry of flow pattern and the validity of heat/mass transfer results. The sidewalls in the test section are removed during these tests to minimize the effect of cross-flow. To ensure the uniform flow at the injection hole exit, the velocity distribution of jet at the hole exit are measured and presented in Fig. 3. The results show good symmetry and uniformity in streamwise direction, and the difference in values near the stagnation regions is within 0.5%. The distributions of Sh along the mid-way ($y/d = \pm 3.0$) at $H/d = 6.0$ have shown a good symmetry in the spanwise direction (within 3% difference of Sh values).

Fig. 4 shows the local Nu distributions obtained by the heat/mass transfer analogy (Eq. (5)) of the present study and other results [8,17] for $H/d = 2.0$ and $Re_d = 10{,}000$. The heat/mass transfer pattern near the stagnation point is affected by the impinging jet flow condition at the hole exit. Therefore, some discrepancies are observed among the results for the same jet Reynolds number. However, at the wall jet region, there is a favorable agreement on the results. In addition, the additional peak values are observed at $r/d = 3.0$ for the array jets due to the interaction between the adjacent wall jets and these values are almost the same for both cases.

3.2. Array impinging jets with/without effusion holes

3.2.1. Flow characteristics

Fig. 5 shows velocity vectors at the center-plane ($y/d = 0.0$) for array impinging jets without effusion holes. For $H/d = 2.0$ (Fig. 5(a)), cross-flow is formed at downstream region and small clockwise vortices are generated at the upstream side of impinging jets due to the interactions between the wall jet flows of adjacent impinging jets and the cross-flow. As the flow moves downstream, flow rate and velocity of cross-flow increase. At $x/d > 18.0$, it is shown clearly that the impinging jets are shifted toward downstream direction. For a large gap distance of $H/d = 6.0$, the effect of cross-flow is reduced because the cross-sectional area increases. The size of vortex near the surface is larger than that for $H/d = 2.0$, and the center of impinging jets are shifted a little.

Fig. 6 presents velocity vectors in the cross-sectional view (y–z plane) at selected planes for the array impinging jets at $H/d = 2.0$. For the cases with cross-flow (Fig. 6(a) and (b)), upward flow at $y/d = \pm 3.0$ (symmetric line) and large-scale vortices are developed due to the collision of wall jets formed from the adjacent impinging jets. As x/d increases, the center of these vortices moves downward and toward the impinging jets. For instance, the center of vortices is located at $y/d \cong \pm 1.8$ and $z/d \cong 1.2$ at $x/d = 0.0$, while the center of vortices is at $y/d \cong \pm 1.5$ and $z/d \cong 1.0$ at $x/d = 24.0$. In addition, the injected jets are more diffused outside near the surface as the flow moves downstream. Therefore, flow re-entrainment of spent air into the injected jet will increase as moving downstream. This reduces the availability of heat transfer performance of the jet due to large mixing of spent air. This is possibly due to the increase of cross-flow rate (velocity) and the development of secondary flow.

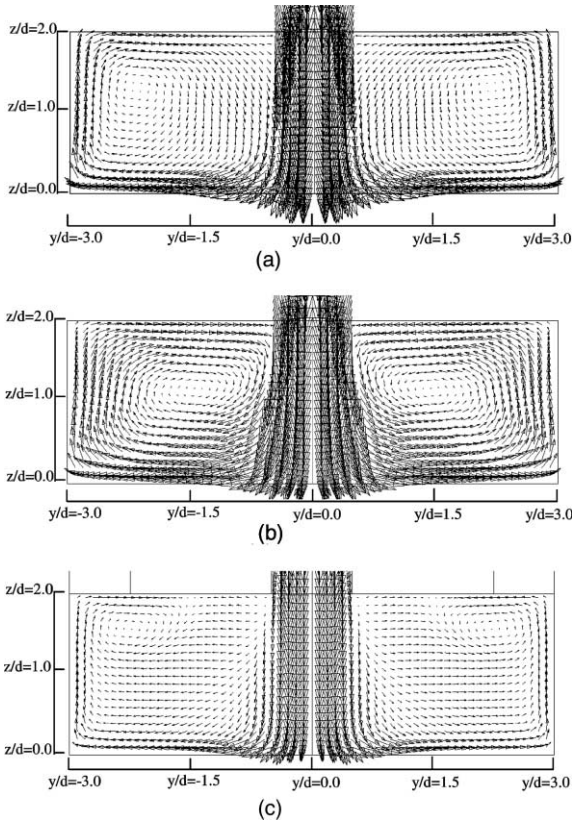

Fig. 6. Velocity vectors at selected planes for array impinging jets without effusion holes at $H/d = 2.0$ and $Re_d = 10{,}000$ (not in scale). (a) $x/d = 0.0$, (b) $x/d = 24.0$ and (c) for array jet with effusion hole.

For the case with effusion holes (Fig. 6(c)), flow pattern at the mid-way region ($y/d = \pm 3.0$) is similar to that with the cross-flow. However, the size of vortices is smaller than that with the cross-flow, and the center of these vortices is located close to the mid-way region (at $y/d \cong \pm 2.3$ and $z/d \cong 1.5$). Hence, the diffusion of the jets and re-entrainment of the spent air are much weaker than those for the case with cross-flow.

3.2.2. Local heat/mass transfer measurements

Fig. 7 shows the contour plots for the array impinging jets without effusion holes at $Re_d = 10{,}000$. For $H/d = 1.0$ (Fig. 7(a)), two peak values are observed near the stagnation region at upstream region ($x/d < 6.0$), which is a typical pattern for impinging jets at small gap distances. At downstream region, asymmetric distributions of *Sh* are formed. The strength of wall jet on the upstream side of stagnation point is weaker than that on the downstream side due to the cross-flow. Therefore, heat/mass transfer enhanced region is shifted toward the downstream side, and the local gradient of *Sh* distribution on the upstream side is very steep, while *Sh* on the downstream side is changed gradually. Local values of *Sh* at the stagnation points increase as x/d increases because turbulence intensity of jet core is elevated due to the interaction between the cross-flow and impinging jets.

While the impinging jet has a little influence on heat/mass transfer rate at mid-way region, heat/mass transfer pattern at this region is much affected by the cross-flow. For the case of $H/d = 1.0$, the flow pattern at the mid-way region is similar to a duct flow at downstream region because of the small spacing between the injection and target plates, and the wall jets of adjacent impinging jets do not interact with each other but flow downstream at this region. Therefore, heat/mass transfer coefficients on the downstream region are lower due to the developed boundary layer, and non-uniform distribution in lateral direction is obtained.

For $H/d = 2.0$, overall heat/mass transfer characteristics are similar to those for $H/d = 1.0$. At downstream region of $x/d > 12.0$, heat/mass transfer enhanced region is spread widely in lateral direction due to the large-scale vortices shown in Fig. 6, and asymmetric distributions are also formed. However, in this case, the effect of cross-flow is weakened due to the

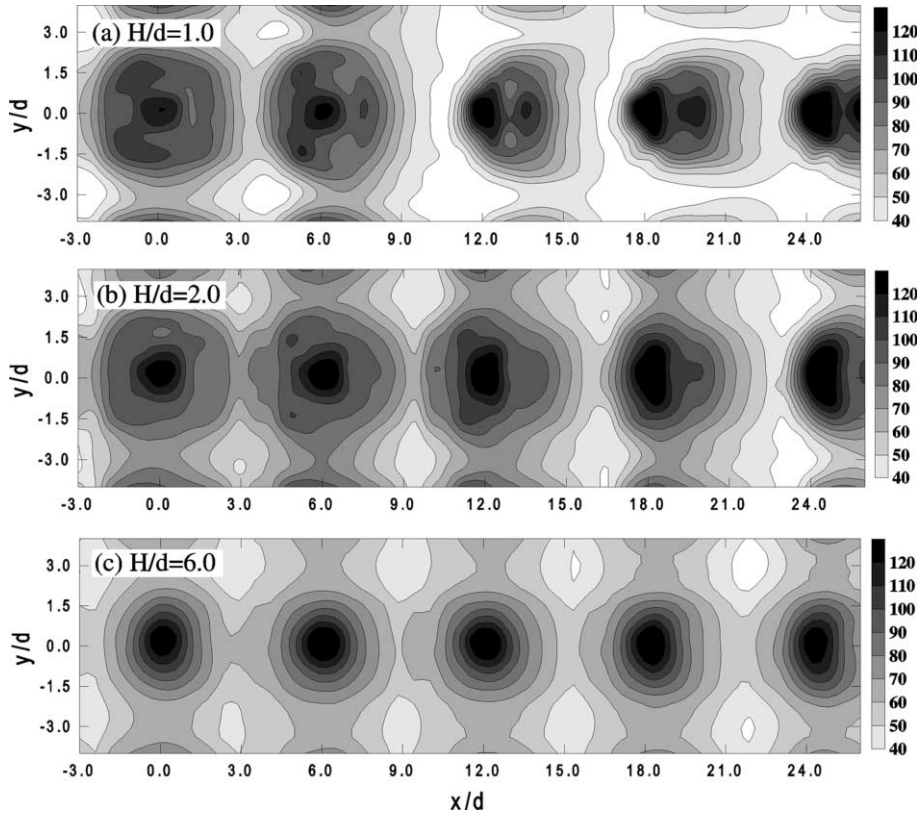

Fig. 7. Contour plots of *Sh* for array impinging jets without effusion holes at $Re_d = 10{,}000$. (a) $H/d = 1.0$, (b) $H/d = 2.0$ and (c) $H/d = 6.0$.

increase of cross-sectional opening area. The local *Sh* on the mid-way region is higher than that for $H/d = 1.0$ because of the interactions between adjacent wall jets.

For a relatively large gap distance ($H/d = 6.0$), the distributions of *Sh* are fairly symmetric in the overall region except at the channel exit region ($x/d \geqslant 24.0$). Heat/mass transfer coefficient reaches a maximum value at the stagnation point and decreases monotonously because the jet potential core remains until this distance with a maximum turbulence intensity [8].

Fig. 8 presents the contour plots of *Sh* for array impinging jets with effusion holes. Dotted circles in the contour plots represent the positions of effusion holes on the injection plate. Symmetric distributions of *Sh* are obtained in the overall region by installing the effusion holes on the injection plate for all the tested cases.

For $H/d = 1.0$, two peak values are observed near the stagnation regions, and square cells of high heat/mass transfer coefficients are formed due to interaction between the adjacent wall jets and flow effusion through the effusion holes. The flow is detached from the surface of target plate and ejection through the effusion holes at the regions where the effusion holes are located. Therefore, upward flow patterns are generated and relatively low transfer regions are appeared at these regions.

As the gap distance increases, the impinging jets become diffused and turbulence intensity of the jet core increases, thus one peak value is observed at each stagnation point. In addition, a large portion of the injected jet is effused through the effusion holes before impinging on the target plate. Therefore, heat/mass transfer coefficients at the mid-way region is lower than those for the small gap.

Local plots of *Sh* for array impinging jets without effusion holes are presented in Fig. 9. For the small gap distances ($H/d \leqslant 2.0$), the cross-flow enhances heat/mass transfer rates at the stagnation region on the target plate with increasing turbulence intensity of the impinging jets. Thus, *Sh* at the stagnation points increases as the fluid moves downstream. For $x/d \geqslant 9.0$, the secondary peak values due to the jet flow transition to turbulence are only formed at the downstream side of the stagnation points because the cross-flow affects the upstream side of the jet. However, there is an apparent decrease of heat/mass transfer at the mid-way region ($y/d = 1.5$ and 3.0) because of development of thermal boundary layer

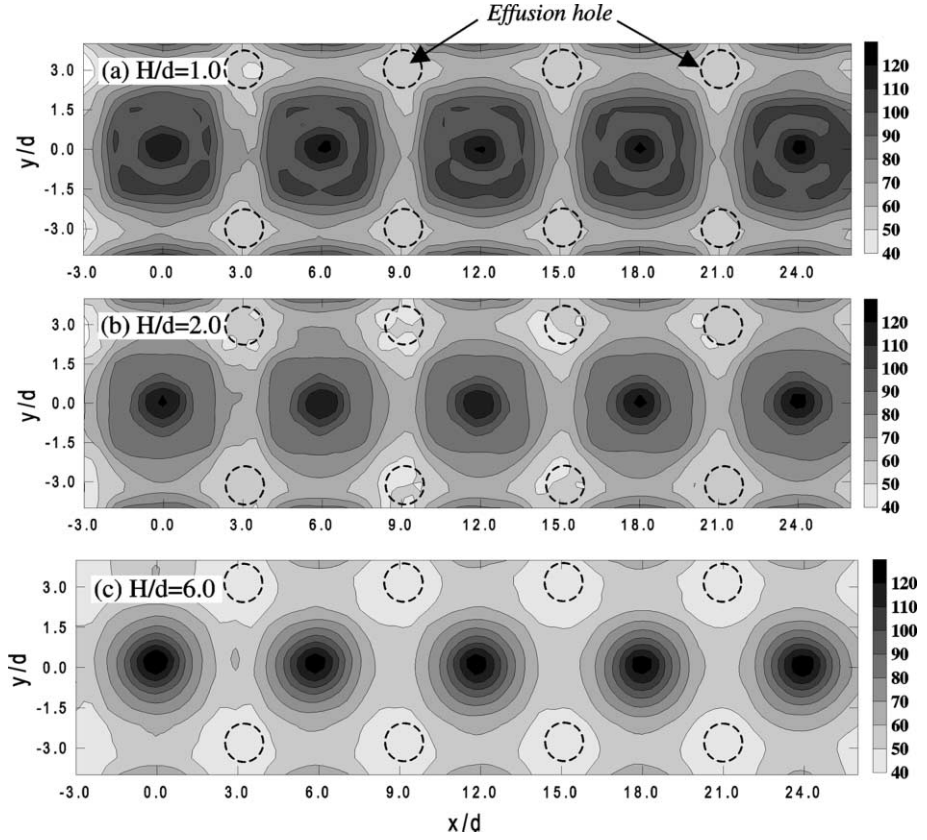

Fig. 8. Contour plots of *Sh* for array impinging jets with effusion at $Re_d = 10{,}000$. (a) $H/d = 1.0$, (b) $H/d = 2.0$ and (c) $H/d = 6.0$.

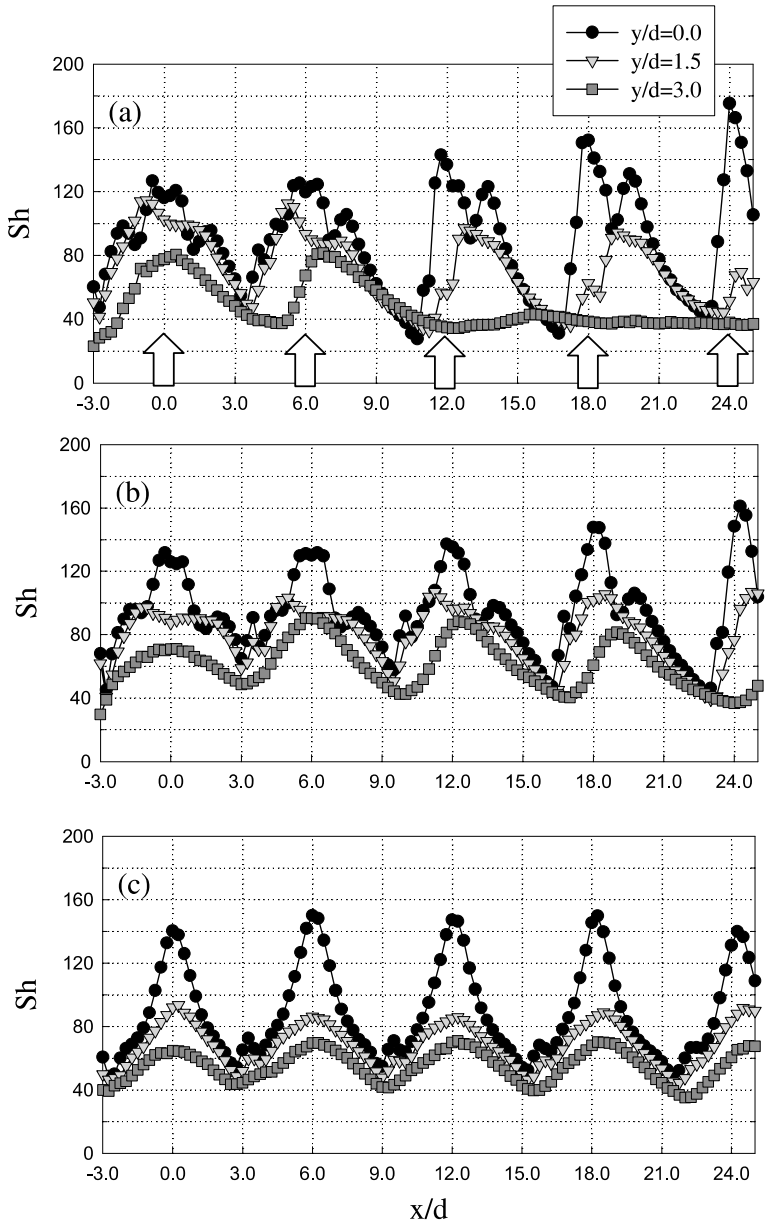

Fig. 9. Local distributions of *Sh* for array impinging jets without effusion holes at $Re_d = 10{,}000$. (a) $H/d = 1.0$, (b) $H/d = 2.0$ and (c) $H/d = 6.0$.

and re-entrainment of the spent air. Therefore, the cross-flow enhances the heat/mass transfer at the stagnation region but reduces that on the mid-way region. For $H/d = 1.0$, the local heat/mass transfer coefficients at the mid-way region stay constantly for $x/d \geqslant 12.0$ because the cross-flow prevents the collisions between the adjacent wall jets. For $H/d = 2.0$, the local distribution at the center-line ($y/d = 0.0$) is similar to that for $H/d = 1.0$. However, at the mid-way region ($y/d = 3.0$), the local heat/mass transfer coefficients at downstream region are higher than those for $H/d = 1.0$ due to the interaction between the wall jets as mentioned before.

For the large gap distances ($H/d \geqslant 4.0$), the distributions of *Sh* are fairly periodic in the overall region because the cross-flow affects heat/mass transfer slightly. Only one peak value is observed at each stagnation point, and the levels of these peak values are similar for all the stagnation points. At the center-line ($y/d = 0.0$),

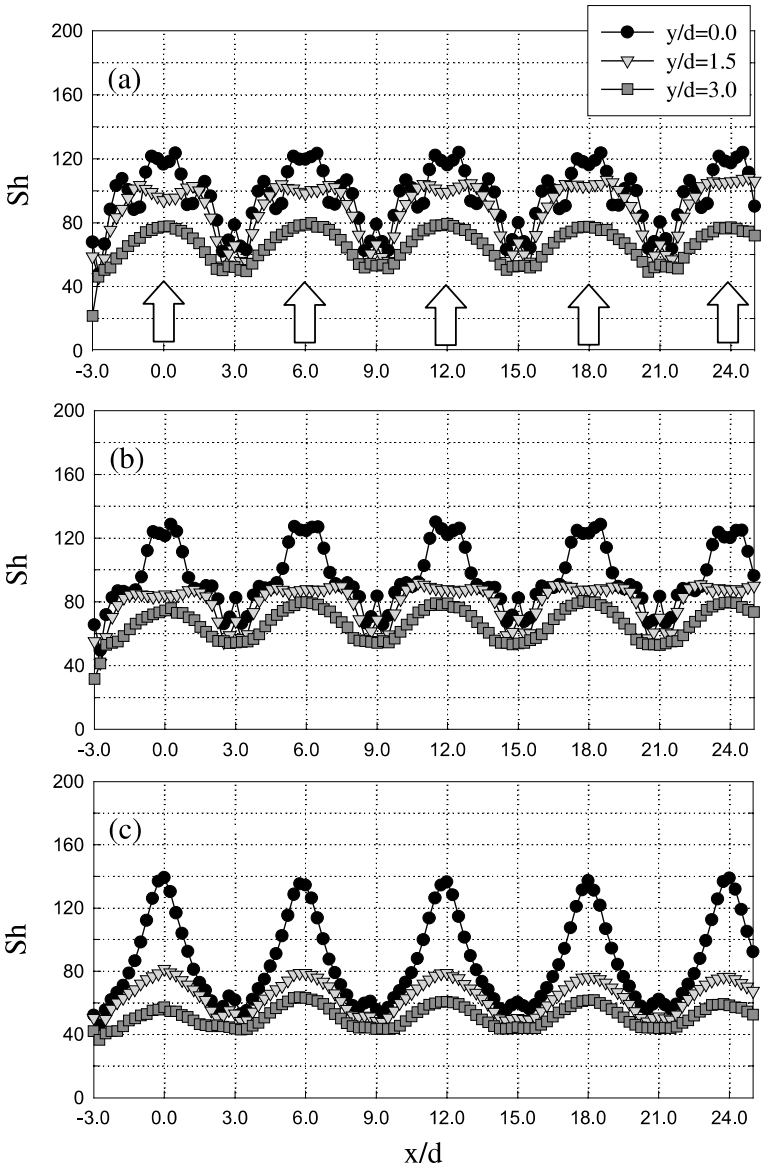

Fig. 10. Local distributions of *Sh* for array impinging jets with effusion holes at $Re_d = 10{,}000$. (a) $H/d = 1.0$, (b) $H/d = 2.0$ and (c) $H/d = 6.0$.

there are additional small peak values between the impinging jets ($x/d \approx 3.5$, 9.5, 16 and 22). This is due to the small clockwise vortices, which are generated through the interaction between the adjacent wall jets as shown in the numerical results (Fig. 5).

Fig. 10 presents local plots of *Sh* for the array impinging jets with effusion holes. The distributions are quite periodic and fairly uniform in the overall region for all the tested cases. There are two peak values at the stagnation region for the small gap distances ($H/d \leqslant 2.0$), but only one peak value is observed for relatively large gap distances due to the development of the jet core flow. The additional small peak values are formed at the midway ($x/d = 3.0$, 9.0, 15.0 and 21.0) due to the interaction between the wall jets. These peak values are decreased as the gap distance increases because the jet is more diffused and the momentum of core flow decreases for the large gap distance.

3.2.3. Average heat/mass transfer coefficient

Fig. 11 shows distributions of laterally averaged *Sh* ($\overline{Sh}$) for the various gap distances at $Re_d = 10{,}000$. For

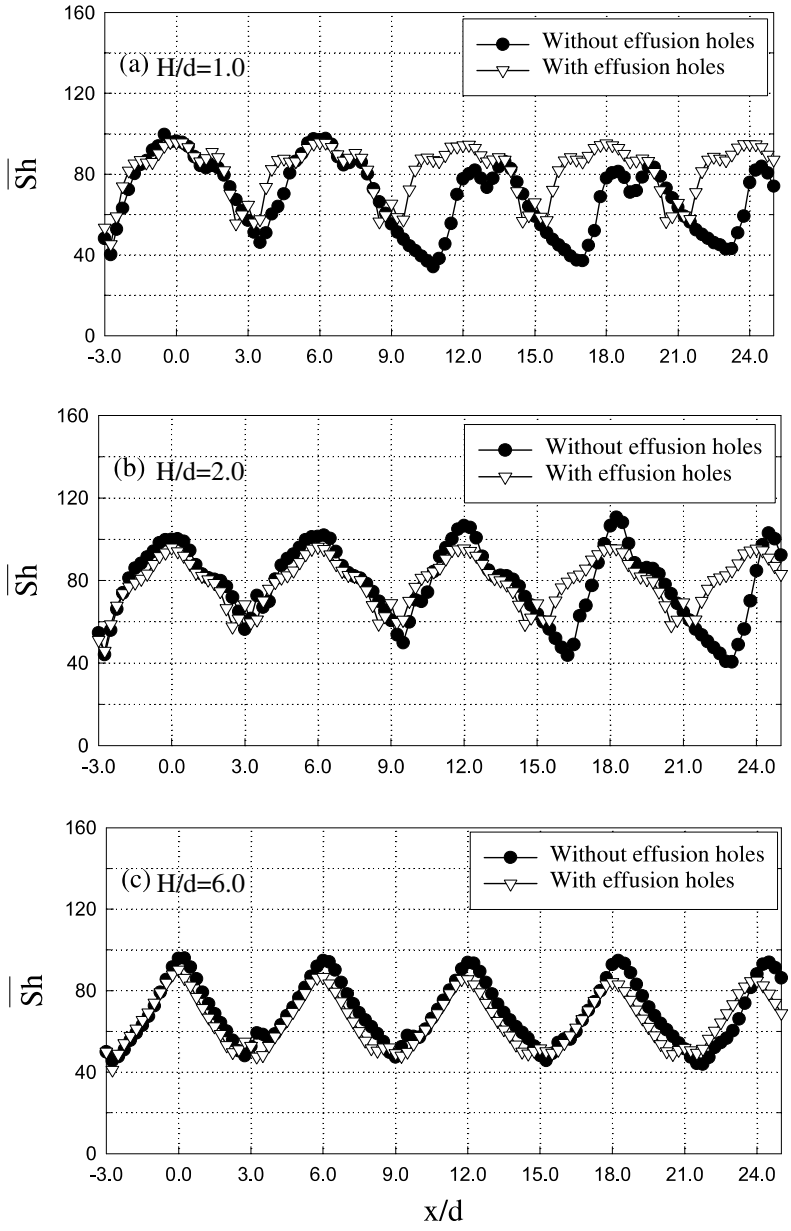

Fig. 11. Local distributions of $\overline{Sh}$ for various gap distances at $Re_d = 10{,}000$. (a) $H/d = 1.0$, (b) $H/d = 2.0$ and (c) $H/d = 6.0$.

the small gap distances ($H/d \leqslant 2.0$), the distribution with the cross-flow is similar to that with the effusion holes at the upstream region ($x/d < 9.0$), but $\overline{Sh}$ values are much less than those with effusion holes at the downstream region due to negative effects of the cross-flow. The negative effects are the re-entrainment of the spent air into the jet and the development of the thermal boundary layer. The difference is larger with the smaller gap distance. For the large gap distance of $H/d = 6.0$, the distributions of two cases, as expected, are almost the same for the overall region. This means that the cross-flow affect little the heat/mass transfer for the large gap distances ($H/d \geqslant 6.0$).

Fig. 12 presents the overall-averaged Sh ($\overline{\overline{Sh}}$) for the various gap distances at $Re_d = 10{,}000$. For the case without effusion holes, the cross-flow has negative effects such as re-entrainment of the spent flow and development of the thermal boundary layer on heat/mass transfer enhancement on the target plate for the small gap distances ($H/d < 2.0$). The maximum value is

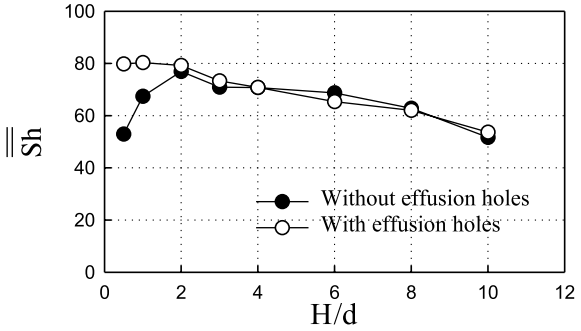

Fig. 12. Overall average Sh for various gap distances at $Re_d = 10{,}000$.

obtained at $H/d = 2.0$, and then $\overline{\overline{Sh}}$ decreases gradually as the gap distance increases. For the case with effusion holes, the spent air in the gap is ejected through the effusion holes. Hence, the cross-flow is not generated and flow re-entrainment is reduced significantly. Thus, $\overline{\overline{Sh}}$ has a maximum value at the small gap distance ($H/d = 1.0$), and this is about 20% higher than the value without the effusion holes. The difference between two cases increases as the gap distance decreases. For $H/d = 0.5$, $\overline{\overline{Sh}}$ with effusion holes is about 60% higher than that without the effusion holes. Therefore, it is concluded that the enhancement of heat/mass transfer and the improvement of uniformity are achieved by installing effusion holes for relatively small gap distances. For relatively larger gap distances ($H/d \geqslant 2.0$), the overall average values are similar to the case of cross-flow because the cross-flow does not affect heat/mass transfer on target plate significantly.

4. Conclusions

Flow and heat/mass transfer characteristics for the array impinging jets with and without the effusion holes are investigated for various gap distances. For the array impinging jets without effusion holes, the cross-flow of spent air has large influence on the heat/mass transfer characteristics on the target plate for the small gap distances of $H/d \leqslant 2.0$. For the small gap distances, the heat/mass transfer coefficients at the stagnation points increase as the flow moves downstream because the turbulence intensity of the jet core increases due to the interaction between the impinging jets and the cross-flow. The heat/mass transfer coefficients at the mid-way region are reduced due to re-entrainment of the spent air and the development of the thermal boundary layer. However, for the large gap distances ($H/d \geqslant 4.0$), the cross-flow affects little the heat/mass transfer on the target plate due to the large cross-sectional area of flow path. The maximum average heat/mass transfer coefficient is obtained at $H/d = 2.0$ for the present geometry.

For the array impinging jets with effusion holes, a periodically uniform heat/mass transfer on the target plate is obtained and the average value increases continuously with decreasing H/d because the spent air is discharged through the effusion holes on the injection plate and the flow re-entrainment is reduced significantly. Therefore, for the small gap distances ($H/d < 2.0$), the heat/mass transfer is augmented significantly and the augmented values are 60% and 20% higher for $H/d = 0.5$ and 1.0, respectively, than those without the effusion holes. However, for the large gap distances, local distributions of heat/mass transfer coefficients and average values with the effusion holes are similar to those without the effusion holes (with cross-flow).

References

[1] R.N. Koopman, E.M. Sparrow, Local and average transfer coefficients due to an impinging row of jets, Int. J. Heat Mass Transfer 8 (1975) 1261–1272.
[2] H. Martin, Heat and mass transfer between impinging gas jets and solid surfaces, Adv. Heat Mass Transfer 13 (1977) 1–60.
[3] S.J. Downs, E.H. James, Jet Impingement Heat Transfer—A Literature Survey, ASME Paper No. 87-HT-35, 1987.
[4] K. Jambunathan, E. Lai, M.A. Moss, B.L. Button, A review of heat transfer data for single circular jet impingement, Int. J. Heat Fluid Flow 13 (1992) 106–115.
[5] R. Viskanta, Heat transfer to impinging isothermal gas and flame jets, Exp. Thermal Fluid Sci. 6 (1993) 111–134.
[6] P.H. Yoon, D.H. Rhee, H.H. Cho, Effects of arrays of impinging jets with crossflow on heat/mass transfer, KSME J. B 24 (2) (2000) 195–203.
[7] H.H. Cho, R.J. Goldstein, Effect of hole arrangements on impingement/effusion cooling, in: Proceeding of 3rd KSME-JSME Thermal Engineering Conference, 1996, pp. 71–76.
[8] H.H. Cho, D.H. Rhee, Local heat/mass transfer measurement on the effusion plate in impingement/effusion cooling system, Trans. ASME, J. Turbomach. 123 (2001) 601–608.
[9] D.H. Rhee, J.H. Choi, H.H. Cho, Flow and heat (mass) transfer characteristics in an impingement/effusion cooling system with crossflow, Trans. ASME, J. Turbomach., in press.
[10] B.R. Hollwarth, L. Dagan, Arrays of impinging jets with spent fluid removal through vent holes on the target surface. Part 1: average heat transfer, Trans. ASME, J. Eng. Power 102 (1980) 994–999.
[11] B.R. Hollwarth, G. Lehmann, J. Rosiczkowski, Arrays of impinging jets with spent fluid removal through vent holes on the target surface. Part 2: local heat transfer, Trans. ASME, J. Eng. Power 105 (1983) 393–402.
[12] A.M. Huber, R. Viskanta, Effect of jet–jet spacing on convective heat transfer to confined impinging arrays of axisymmetric air jets, Int. J. Heat Mass Transfer 37 (18) (1994) 2859–2869.

[13] R.J. Goldstein, H.H. Cho, A review of mass transfer measurement using naphthalene sublimation, Exp. Thermal Fluid Sci. 10 (1995) 416–434.
[14] D. Ambrose, I.J. Lawrenson, C.H.S. Sparke, The vapor pressure of naphthalene, J. Chem. Thermodyn. 7 (1975) 1173–1176.
[15] E.R.G. Eckert, Analogies to heat transfer processes, in: E.R.G. Eckert, R.J. Goldstein (Eds.), Measurements in Heat Transfer, Hemisphere Publisher, New York, 1976, pp. 397–423.
[16] S.J. Kline, F. McClinetock, Describing uncertainty in single sample experiments, Mech. Eng. 75 (1953) 3–8.
[17] J.H. Lee, S.J. Lee, Turbulent heat transfer characteristics in a stagnation region of axi-symmetric jet impingement, in: Proceedings of 11th IHTC, vol. 5, 1998, pp. 433–438.